# Fast Proton Hopping Detection in Ice I$_h$ by Quasi-Elastic Neutron Scattering

Itay Presiado,[†] Jyotsana Lal,[‡] Eugene Mamontov,[§] Alexander I. Kolesnikov,[§] and Dan Huppert[†,*]

[†]Raymond and Beverly Sackler Faculty of Exact Sciences, School of Chemistry, Tel Aviv University, Tel Aviv 69978, Israel

[‡]Materials Science Division, Argonne National Laboratory, 9700 South Cass Avenue, Argonne, Illinois 60439, United States

[§]Neutron Scattering Sciences Division, Oak Ridge National Laboratory, Oak Ridge, Tennessee 37831, United States

S *Supporting Information*

ABSTRACT: Quasi-elastic neutron scattering was employed on samples of HCl-doped polycrystalline ice I$_h$. The analysis of the scattering signal provides the excess proton hopping time, τ_{hop}, in the temperature range of 140—195 K. The hopping time strongly depends on the temperature of the sample, and the activation energy of a hopping step is 17 kJ/mol. The values of τ_{hop} of the current experiment are in good agreement with calculated values derived from previous photochemical experiments,[1] in which we found that the proton hopping time at $T > 242$ K is on the order of 200 fs, roughly 10 times shorter than in liquid water at room temperature.
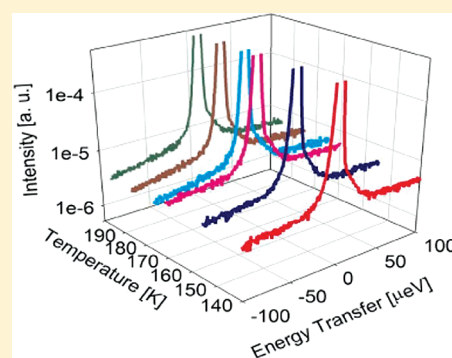
INTRODUCTION

In spite of the fact that the physics of ice[2−5] has been studied extensively for a long time, there are numerous questions left unanswered even to this day.[3] Over the years, ice has challenged many physicists and chemists, and the discoveries they make in this field have global implications. Recently, ice studies revealed the importance of ionization of hydrochloric acid on stratospheric ice particles as a key step in the depletion of the stratospheric ozone.[6] Imperfections in the ice lattice give rise to electrical conduction, defects, diffusion, and dielectric relaxation phenomena. Pure ice exhibits a high static relative permittivity, which is larger than that of liquid water. There are two types of structural defects that are largely responsible for the electrical properties of ice: 1) Ion defects, which are the result of proton motion from one end of the hydrogen bond to the other, thus creating a H$_3$O$^+$, OH$^-$ ion pair.[7] Conduction is then carried out by means of successive proton jumps (the von Grotthuss mechanism). 2) Bjerrum defects,[8] which are orientational defects caused by the rotation of a water molecule to produce either a doubly protonated bond (D-defect) or a deprotonated bond (L-defect). Nowadays, quantum-mechanical ab initio calculations and dynamical simulations present an efficient way to study ion defects,[9] Bjerrum defects[10] and the mechanism of proton transfer and mobility in ice.

Eigen and co-workers conducted electrical conductivity measurements in the 1960s that led them to the conclusion that the proton mobility in pure ice is 10—100 times larger than in water.[11,12] In numerous further measurements by other groups, it was found that at about 263 K the proton mobility in ice (0.8×10^{-4} cm^2 V^{-1}s^{-1}) is smaller than in water[13] by about a factor of 2 (when compared to supercooled liquid water[14,15] at the same temperature). The large proton conductivity of ice found in Eigen's experiments was explained as arising from large surface conductivity rather than from bulk conductivity.[4] Onsager and Runnels[16] and later on Nagle[17] advocated larger values of proton diffusion in ice, however, in the 1972 ice conference in Ottawa, Onsager, Engelhardt and others abandoned the idea of ice as an intrinsic protonic semiconductor.[4]

The effect of HCl adsorption on thin film ice I$_h$ was studied by neutron diffraction[18] and quasi-elastic neutron scattering in the temperature range of 190—270 K. It was found that below 220 K the sample structure is frozen and immobile. Translational mobility, which is a signature of the liquid phase, is observed at 250 K.

In recent years, surface scientists conducted low-temperature studies of proton diffusion in thin film, grown by controlled methods at vacuum conditions. These experiments, which produced interesting results, can be performed only at temperatures below 140 K. The thin film experimental results suggest that protons are mobile through the ice film in both amorphous ($T < 140$ K) and crystalline phases ($T \geq 140$ K) that form during the course of the temperature ramp. Kang[19] suggests that the anomalous experimental reports on the mobility of protons in ice films[20−26] can be explained by the affinity of protons for the ice surface and the facile proton transport near the surface at

$T \geq 130$ K. The result verifies that protons are mobile in an ice film and at favorable temperatures can migrate from the film interior to the surface. This conclusion is unaffected by the changes in ice film morphology and thickness (2−8 BL) and by the presence of counteranions. An extrapolation of Takei and Maeno's HCl-doped bulk ice conductivity data[27,28] until about 140 K indeed shows lower proton conductivities by roughly 7 orders of magnitude than at $T > 250$ K.

In a recent study,[1] we used time-resolved emission measurements to monitor the fluorescence quenching of flavin mononucleotide (FMN) in methanol-doped ice by excess proton over the large temperature range of 80−260 K. We analyzed the time-resolved emission data using the irreversible Smoluchowski model[29] that accounts for both the proton diffusion and reaction with the excited FMN or riboflavin target molecules. A detailed description and analysis of the method are given in the Supporting Information. The analysis provides the proton diffusion coefficient, D_{H^+}, in ice over the large range of temperatures studied. The plot of D_{H^+} as a function of $1/T$ has a complex shape. In general, the temperature behavior of D_{H^+} can be divided into three regions:

a The high-temperature region, $T > 242$ K, in which the temperature dependence is weak and the proton diffusion coefficient is large. The proton diffusion coefficient in this region is $\sim 10^{-3}$ cm^2/s, which is 10 times larger than in water at 295 K, and the activation energy is relatively small, that is, $E_a < 1000$ J/mol (~ 0.01 eV). This value is in good agreement with the proton mobility calculations of Pang and co-worker based on a soliton model, where an ionic defect appears as a solitary wave in the proton sublattice.[30]

b The intermediate-temperature range, 175−242 K, in which the proton diffusion coefficient strongly depends on the temperature. The proton diffusion coefficient deduced from the diffusion-controlled rate coefficient decreases by about a factor of 100 from its value of $\sim 10^{-3}$ cm^2/s at 260 K to $\sim 10^{-5}$ cm^2/s at 175 K. The activation energy of the proton diffusion is large, that is, $E_a = 22$ kJ/mol (0.23 eV).[1]

c The low-temperature region, 80−175 K. In this temperature range, the reaction rate of the proton with FMN is slower than the radiative rate of FMN. The 4 mM HCl sample shows a somewhat shorter decay time of the emission signal than that of an acid-free sample. The proton diffusion coefficient derived for that sample is $\sim 10^{-5}$ cm^2/s. It is almost temperature independent throughout the low-temperature region.

In the current study quasi-elastic neutron scattering (QENS) was used to measure the proton hopping time, τ_{hop}, in HCl-doped ice samples in the temperature range of 140−195 K. The values of τ_{hop} are in good correspondence with the calculated values derived from the photochemically measured proton diffusion coefficient, D_{H^+}, for a random walk model with an average hopping distance of 2.75 Å, which is the distance between oxygen atoms of two adjacent water molecules.

■ RESULTS

The liquid solutions were loaded in the standard cylindrical sample holders of annular geometry, 29 mm in diameter and 0.05 mm thick. The sample thickness was selected to minimize the effects of multiple scattering. The initial cooling of the liquid samples to low temperatures was rapid. We used 1 and 0.1 M HCl samples in this experiment. Starting at room temperature, we first cooled the samples down to 5 K in about two hours, and then measured the resolution at 5 K for some 4 h. Subsequently, we warmed up the samples to 140 K (in case of the 1M) and 175 K (in case of the 0.1 M) and continued with the temperature-dependent measurements. The temperature of the samples was kept constant with an accuracy of 0.2 K throughout the measurement. The experiment was performed on the backscattering spectrometer, BASIS, at the Spallation Neutron Source, Oak Ridge National Laboratory, USA.[31] A dynamic range of energy transfers of $\pm 100 \, \mu$eV was used for the data analysis, whereas the energy resolution (averaged over the entire accessible range of the momentum transfer, 0.2 Å^{-1} < Q < 2.0 Å^{-1}) was about 3.5 μeV, fwhm. Thus, the dynamic processes on the approximately 6−400 ps time scale and 3 −30 Å length scale were probed.

In a QENS experiment, the inelastic scattering intensity is measured as a function of the neutron energy transfer,

$$E = E_i - E_f = (h^2/2m)((1/\lambda_i)^2 - (1/\lambda_f)^2) \quad (1)$$

and scattering momentum transfer,

$$Q = ((2\pi/\lambda_i)^2 + (2\pi/\lambda_f)^2 - 2(2\pi/\lambda_i)(2\pi/\lambda_f) \cos 2\theta)^{1/2} \quad (2)$$

where h is the Planck constant, m is the neutron mass, λ_i and λ_f are the initial and final neutron wavelengths respectively, and 2θ is the scattering angle. For small energy transfers (near-elastic scattering), when $\lambda_i \approx \lambda_f \approx \lambda$, the scattering vector becomes simply $Q \approx 4\pi \lambda^{-1} \sin \theta$. Accurate measurements of the scattering intensities at very small energy transfers near the elastic line require high energy resolution; thus, dedicated spectrometers such as the BASIS are often used for QENS experiments.

For a sample that exhibits no diffusion dynamics on the time (that is, the energy resolution) scale of the QENS measurement, the scattering intensity is purely elastic and represents the resolution function of the spectrometer. Examples of elastically scattering samples include a vanadium standard and samples measured at very low temperatures, where the diffusion mobility either ceases or becomes too slow for the spectrometer resolution. When the mobile species in the sample move sufficiently fast to yield signal broadening beyond the elastic line, this broadening is often fit with a Lorentzian, which is a Fourier-transformation into the energy space of an exponential function that represents the time-dependent decay of the self-correlation function of the diffusing particle in the time space. It should be noted that the scattering from hydrogen-bearing samples is usually dominated by the hydrogen due to its very large incoherent neutron scattering cross-section compared to other elements. Thus, measurements of such samples mostly yield information on single-particle diffusion of the present mobile hydrogen-bearing species. If both mobile or immobile (or too slow) species coexist in the sample, then the scattering signal is a superposition of the elastic and quasielastic (that is, broadened beyond the resolution) contributions.

The scattering intensity as a function of the energy transfer, E, was fit using the following customarily used expression:

$$I(E) = \left[x\delta(E) + (1 - x)\frac{1}{\pi}\frac{\Gamma}{\Gamma^2 + E^2} \right] \otimes R(E) + (C_1 E + C_2) \quad (3)$$

which includes a superposition of the delta-function centered at zero energy transfer (the elastic line) and a Lorentzian-shaped quasielastic broadening convolved with the resolution function, $R(E)$, plus a linear background. The latter originates from both the processes that are too fast on the experiment time scale
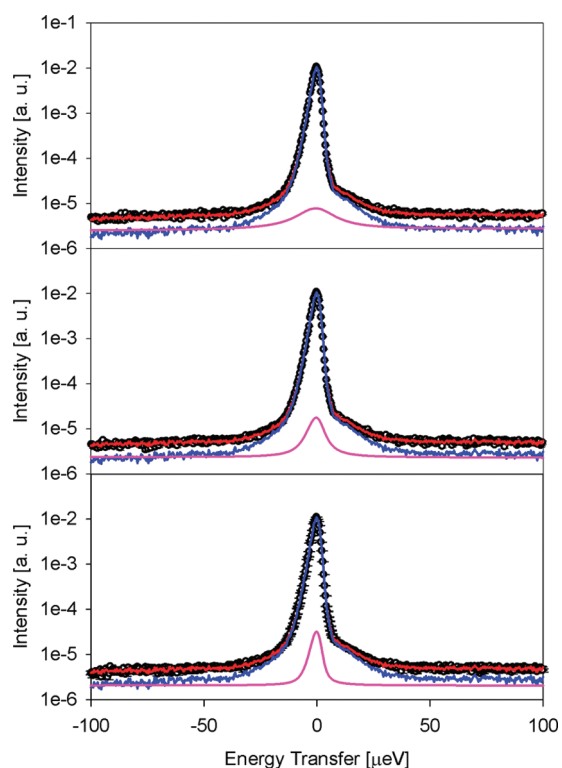
10246

dx.doi.org/10.1021/jp2008094 |J. Phys. Chem. C 2011, 115, 10245−10251

Figure 1. Quasi-elastic neutron scattering signals of ice sample doped with 1 M of HCl at 140 (bottom), 155 (middle), and 170 K (top). Symbols, data; red line, overall fit; blue line, elastic fit component; pink line, quasielastic fit component and fit background.

Figure 2. Quasi-elastic neutron scattering signal of ice sample doped with 0.1 M HCl at 175 (bottom), 185 (middle), and 195 K (top). Symbols, data; red line, overall fit; blue line, elastic fit component; pink line, quasielastic fit component and fit background.

(if there are any) and the measurement background. The resolution function that we used was collected from each respective sample at the baseline temperature of about 5 K, where all possible diffusion motions cease and the scattering becomes purely elastic.

In principle, one of the biggest advantages of QENS as a technique is its capability of extracting the information regarding the geometry of diffusive motions through the Q-dependence of the fit parameters. Unfortunately, in this work, we were unable to analyze the data at separate Q values and had to use Q-averaged data instead. This was because of the extremely weak fraction of the quasielastic signal in the total spectra; the parameter x in the fits with eq 3 ranged between 0.9882 and 0.9988. The scattering was overwhelmingly elastic, suggesting that only a very small fraction of the protons in the samples exhibited mobility on the experiment time scale. The difficulties in extracting very weak quasielastic contribution from the data fits precluded the Q-dependent analysis of the data, which, in principle, could provide information of the proton jumps geometry. Instead, the diffusion jump times were obtained from the HWHM of the Q-averaged Lorentzian broadening, Γ, in eq 3, as $\tau_{hop} = \hbar/\Gamma$.

In fact, fitting the very weak quasielastic signal in the presence of the overwhelmingly strong elastic signal was only possible because of the excellent signal-to-noise ratio of the BASIS at the elastic line of several thousand to one.[31]

Figure 1 shows the quasi-elastic neutron scattering signals of ice sample doped with 1 M of HCl, which is considered a relatively high concentration, at 140, 155, and 170 K. Figure 2 shows the QENS signal of ice sample doped with the relatively low HCl concentration of 0.1 M at 175, 185, and 195 K.
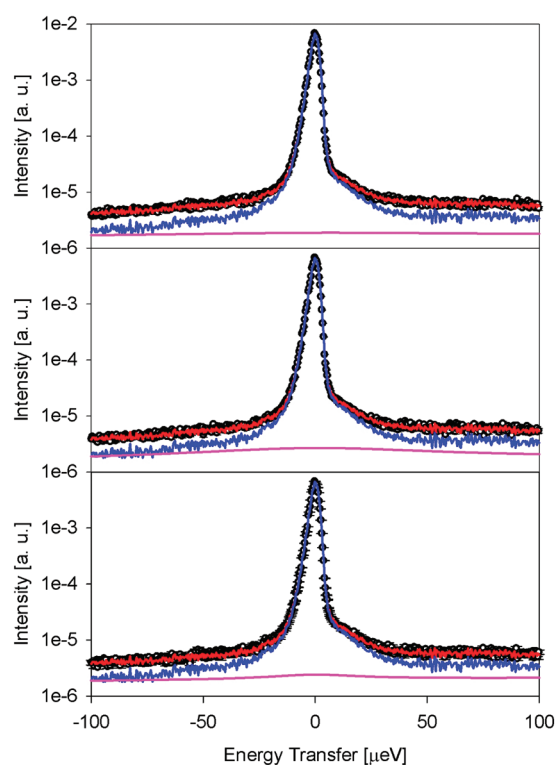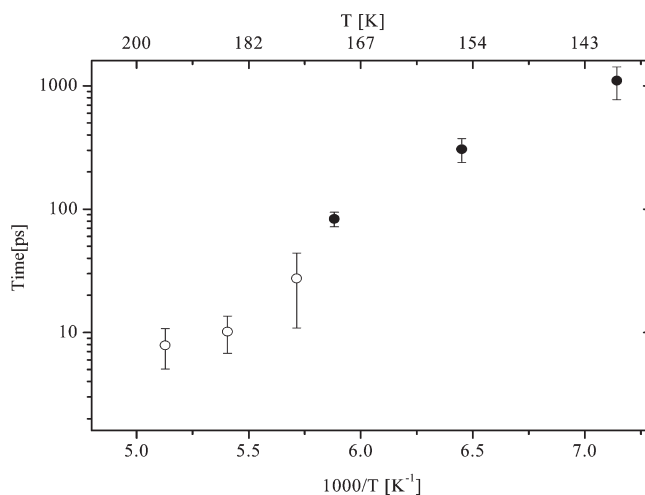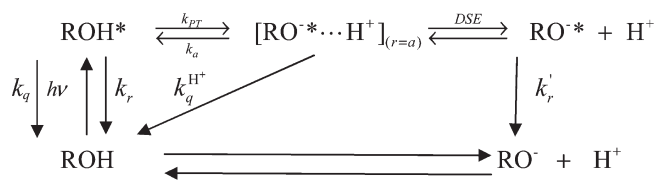

Figure 3. Arrhenius plot of the proton hopping times derived from the QENS measurements versus $1000/T$. Full circles, 1 M HCl; empty circles, 0.1 M HCl.

Figure 3 shows the proton hopping time versus $1000/T$ (an Arrhenius plot). The hopping times strongly depend on the temperature: the lower the temperature the longer the hopping time becomes. The three data points at the lowest temperatures were measured with a 1 M HCl sample. The hopping times are 83, 305, and 1100 ps for 170, 155, and 140 K, respectively. The activation energy for the three data points is 17 kJ/mol. At three higher temperatures, the neutron scattering signals were

10247

dx.doi.org/10.1021/jp2008094 |*J. Phys. Chem. C* 2011, 115, 10245–10251

Scheme 1

$$\text{ROH*} \underset{k_a}{\overset{k_{PT}}{\rightleftarrows}} [\text{RO}^{-*}\cdots\text{H}^+]_{(r=a)} \underset{}{\overset{DSE}{\rightleftarrows}} \text{RO}^{-*} + \text{H}^+$$

$$k_q \Big\downarrow \, hv \quad \Big\downarrow k_r \quad k_q^{H^+} \qquad \qquad \qquad \Big\downarrow k_r'$$

$$\text{ROH} \qquad \qquad \longrightarrow \text{RO}^- + \text{H}^+$$

collected from an ice sample doped with 0.1 M of HCl. At this low concentration, the quasielastic scattering signal is even weaker in comparison with signal of the elastic neutron scattering from bulk H_2O ice. Also, the width of the neutron scattering signal is large, since the hopping time is short at the relatively high temperatures of 175, 185, and 195 K.

Even given the excellent capabilities of the BASIS, the quasielastic signals, especially those collected for the 0.1 M HCl sample, were on the borderline of the spectrometer sensitivity, as evidenced by the relatively large error bars in the higher-temperature relaxation times presented in Figure 3.

Photochemical Experiment. In this type of experiment, we dope the ice sample with three dopants. We add low concentrations of inorganic acid and of an organic molecule that reacts with a proton in its electronically excited state in both ice and liquid water. Moreover, we add 0.2% mole ratio of methanol as a cosolvent that prevents the expulsion of the relatively large photochemical molecule from the bulk ice. Without the addition of methanol the fluorescence intensity of the photoreactive organic molecule is reduced by 2 orders of magnitude or more, depending on the type of the molecule. The amphiphilic properties of methanol make it a suitable mediator between the water molecules and the largely hydrophobic active molecules. The methanol prevents the expulsion of the organic molecules to the grain boundaries. FMN and other photoactive molecules used in previous experiments[1,32,33] are termed photoacids and photobases. When a proton reaches a photoacid in its deprotonated form, termed RO^{-*}, it can recombine with it to form the excited protonated photoacid, ROH*, or the ground-state protonated photoacid ROH(g). Scheme 1 illustrates the two reactions of proton recombination as well as the excited-state proton transfer (ESPT) taking place prior to the recombination process.

k_{PT} and k_a are the intrinsic proton transfer and proton recombination rate constants, respectively. The proton recombination process is determined by the proton diffusion coefficient and the Coulomb attraction potential between the negatively charged deprotonated RO^{-*} form and the proton. The accurate time dependent size of the ROH* and RO^{-*} species populations can be determined by using the Debye–Smoluchowski equation (DSE) with appropriate initial and boundary conditions.[34] A more detailed description of Scheme 1 is given in refs 21 and 22.

Irreversible photoacids are photoacids whose deprotonated RO^{-*} form's lifetime decreases as the acid concentration increases in both liquid and ice. The molecule we used for observing the reaction rate of a proton in ice is flavin mononucleotide (FMN). The excited-state lifetime of FMN in neutral pH in liquid H_2O and ice is 5.4 ns. In a 2 mM solution of HCl, the lifetime slightly reduces to ~5 ns in liquid, whereas in ice it dramatically reduces to about 1 ns. We attribute this large difference between the fluorescence lifetimes of FMN in liquid and in ice to the large proton diffusion coefficient of the latter.
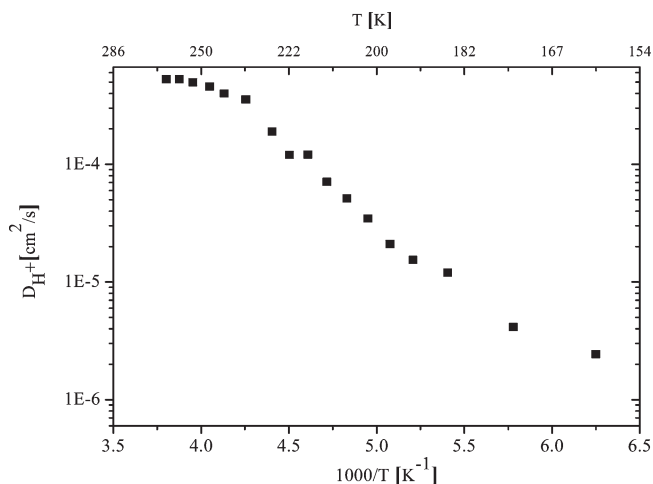

Figure 4. Proton diffusion coefficient in ice doped with 1 mM HCl measured by photochemical methods, $D_{H^+}^{ice}$, versus $1000/T$ in the range of 140–265 K.

The binary collision reaction of two species, say A and B, where reactant B is in large excess over A, to form a product C depends on the mutual diffusion process, bringing the two reactants to a contact distance. In ice the protons (compound B) are mobile, whereas the photoacid is stationary. The overall reaction rate depends on both, the intrinsic contact reaction rate constant, k_a, and the diffusion-controlled rate constant, k_D. When $k_a > k_D$ the diffusion-controlled reaction rate constant determines the overall reaction rate constant. Thus, the proton diffusion in ice is evaluated from the reaction of protons with FMN in the methanol-doped ice sample.

Figure 4 shows the plot of proton diffusion coefficient in ice, $D_{H^+}^{ice}$ versus $1/T$. $D_{H^+}^{ice}$ was deduced from the excited-state emission decay of FMN in ice I_h doped with 2 mM of HCl at several temperatures in the range of 88–265 K. As mentioned in the introduction, in Figure 4 we can observe three regions, in which $D_{H^+}^{ice}$ behaves distinctly. At 242 K or higher, $D_{H^+}^{ice}$ has a high value, and it is nearly temperature independent. In experiments, in which we used 0.1% mole ratio of methanol, which is half of the amount used in the samples shown in Figure 4, we find that $D_{H^+}^{ice}$ is 10 times greater than in liquid water at room temperature, that is, $D_{H^+}^{ice} = 1 \times 10^{-3} \text{cm}^2/\text{s}$. The value of $D_{H^+}^{ice}$ is nearly inversely proportional to the methanol concentration, that is, at concentration of 0.2% mole, $D_{H^+}^{ice}$ value is halved. In the temperature range of 175–242 K, $D_{H^+}^{ice}$ decreases with the temperature decrease, and its activation energy is ~22 kJ/mol. At temperatures below 175 K, the value of $D_{H^+}^{ice}$ is 2 orders of magnitude smaller than at $T > 242$ K. The residual value of ~10^{-5} cm^2/s is almost temperature independent. We attribute this value to protons trapped in the immediate vicinity of FMN molecules. It is important to note that the ice structure around FMN molecules is far from that of the ordered I_h crystal structure. Alternatively, a proton may reside on a phosphate group of FMN, whose pK_a value is ~3 at room temperature. Protonated phosphate can easily release the proton that can then react with the excited flavin moiety, and consequently decrease the accuracy of calculation of $D_{H^+}^{ice}$ at $T < 175$ K. The contribution of the low-temperature $D_{H^+}^{ice}$ of about 10^{-5} cm^2/s was subtracted from the experimental data shown in Figure 4.
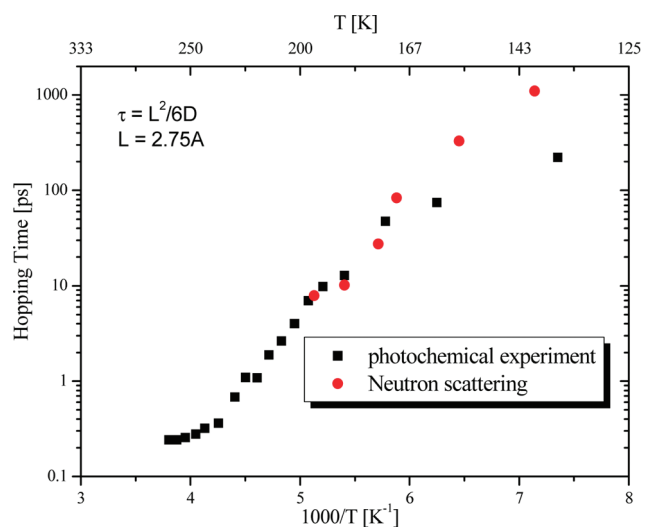
Figure 5. Hopping times of protons in HCl doped ice obtained from two types of experiments, the quasi-elastic neutron scattering (full circles), and the previously reported photochemical experiments (full squares).

Analysis of the Proton Diffusion Data. We used the Einstein relation given below to calculate the hopping time of a diffusing particle:

$$\tau_{hop} = \langle L^2 \rangle / 6D \qquad (4)$$

where L is the average hopping distance and D is the diffusion coefficient of the particle. In ice I_h the distance between oxygen atoms of adjacent water molecules is 2.75 Å. The proton moves from one water molecule to the nearest neighbor along the ice structure,[5] and therefore $L = 2.75$ Å is conceivable. Squared points in Figure 5 show the hopping time of a proton in ice derived indirectly from the photochemical experiment plotted versus $1/T$. In the high-temperature region, $D \approx 5 \times 10^{-4}$ cm^2/s and $\tau_{hop} \approx 250$ fs. The value of D decreases and the proton hopping time increases as the temperature decreases. At 150 K, the hopping time increases by 3 orders of magnitude until it reaches a value of ~250 ps.

Figure 5 juxtaposes the hopping time of protons in ice derived from two types of experiments, the neutron scattering experiment (Figure 3, full circles) and the previously reported photochemical experiments (squares). As seen in Figure 5, the proton hopping times of the two types of experiments in the temperature range of 150−195 K are in rather good agreement. To get a better agreement between the τ_{hop} values of the two experiments, we used an additional adjustable parameter that multiplies the τ_{hop} values derived from the photochemical experiments, $\tau_{hop} = a \cdot \tau$. We find that the best match between the two sets of data is achieved when the value of a is about 1.5. The photochemical data provides after some analysis the value of $D_{H^+}^{ice}$. The proton hopping time is calculated by using eq 4, describing a 3D random walk. The value of the distance between two adjacent oxygen atoms in ice I_h was used in L for the purpose of this calculation. The adjustable parameter may suggest that the average distance is somewhat longer than 2.75 Å, i.e., $L = (a)^{1/2} \times 2.75 \approx 3.4$ Å. It was suggested in the literature that proton diffusion proceeds via a Grotthuss-like mechanism, in which a single proton is not really hopping along a water molecule chain but rather hops only a

single step to the nearby water molecule. Another proton from the newly formed H_3O^+ species is released and hops to the nearest adjacent water molecule and so on. Such a proton shuttle mechanism is more effective because in ice the initiator proton cannot propagate prior to a water molecule rotation of 120°. The Grotthuss mechanism may account for the fact that the effective average combined step is longer than 2.75 Å.

In the past,[1] we suggested a stepwise model to account for the complex temperature dependence of the proton diffusion coefficient. We describe below an oversimplified model calculation for the purpose of obtaining a qualitative description of the temperature dependence of the experimental proton diffusion constant in ice. The model restricts the proton transfer process to be stepwise. The proton moves to the adjacent water molecule only when the hydrogen alignment of the water molecule brings the system to the lowest energy barrier of the proton coordinate. In the stepwise model, the overall proton transfer time is a sum of two times, $\tau = \tau_s + \tau_H$, where τ_s is the characteristic time for the hydrogen orientation of the water molecule, and τ_H is the time for the proton to pass over or under the barrier of the double well curve describing the potential along the axis between the two oxygen atoms properly aligned in the hexagonal ice structure. The overall rate constant $k(T)$ at a given T is

$$\frac{1}{k(T)} = \frac{1}{k_H(T)} + \frac{1}{k_s(T)} \qquad (5)$$

where k_s is the hydrogen reorientation coordinate rate constant, and k_H is the proton coordinate rate constant. Similar expressions for an overall rate constant are used for several important phenomena such as the overall rate constant for the electron transfer rate,[35] and a diffusion-assisted chemical reaction.[36,37] Eq 5 provides the overall proton transfer rate constant along the lines of a stepwise process similar to the processes mentioned above. As a solvent coordinate rate constant in liquid water, we used $k_s = b(1/\tau_D)$, where b is an adjustable empirical parameter. In previous studies on liquids, we found that the empirical factor for water is about 8. Thus, the orientational characteristic time $\tau_s = 1.0$ ps. In ice, the diffusion constant for the L-defect, D_L, is associated with a hydrogen rotation about the oxygen−oxygen axis along the hexagonal structure of the ice, where the oxygen atoms are at the vertices.

The reaction rate constant k_H along the proton coordinate is expressed by the usual activated chemical reaction description given by eq 6. At high temperatures, the orientational relaxation of the hydrogen alignment is fast, and thus the rate-determining step is the actual proton transfer coordinate

$$k_H = k_H^0 \exp\left(-\frac{G_a^H}{RT}\right) \qquad (6)$$

where k_H^0 is the preexponential factor determined by the fit to the experimental results, and G_a^H is the activation energy determined by the slope of the Arrhenius plot in the high-temperature region of $D_{H^+}(T)$ above 235 K, where $k_s > k_H$, and the rate constant of the determining process is k_H.

Temperature Dependence of τ_s in Ice. The frequency dependence of the dielectric constant in ice provides the Debye relaxation time, τ_D, which is relatively short in liquid water, that is, 8 ps at 20 °C. It is determined by the polarization frequency dependence and should not be mistaken with a single water molecule's rotation time, which is roughly 1 ps at room temperature.

τ_D in ice at 253 K is about 7 orders of magnitude longer than in liquid water, $\tau_D^{ice} = 1.4 \times 10^{-4}$s. τ_D in ice is related to a single water molecule's rotation about the oxygen–oxygen axis and is given by:

$$\frac{1}{\tau_D^{ice}} = \frac{n_L \nu_L}{3N} \qquad (7)$$

where n_L and N are the number of L-defects and water molecules per unit of volume, respectively. The reorientation time τ^L associated with the dielectric relaxation in ice is the reciprocal of υ_L. Given the value of τ_D in ice and that the n_L/N is roughly $\sim 10^{-7}$ at high-temperature ice, the estimated value of τ^L is 3×10^{-12}s. This value is about 10 times slower than the hopping time deduced from the proton diffusion coefficient (Figures 4 and 5). The rotation of the water molecule in liquid is also 10 times faster than τ_D. An interesting point to note is that the activation energy of the L-defect is 20 kJ/mol,[38] which is about the same value as obtained from the data shown in Figure 5 for low-temperature proton hopping time. In conclusion, proton hopping time in ice at $T < 235$ K may be limited by the reorientation time of a water molecule. This mechanism also applies to the dielectric relaxation of ice and to the proton and L-defect mobilities in ice.

Why is the Neutron Scattering Experiment Important? Ice is known to be a poor solvent of ionic compounds and especially of large organic molecules. Frozen liquid water forms micrometer sized polycrystalline ice I_h. The question that arises then is where are all the dopant molecules positioned in the sample? A large fraction of the organic molecules may be expelled and aggregate at the grain boundaries. In extreme cases, all of the dopant molecules, the photoacid, HCl, and methanol are aggregated at the grain boundaries. The photochemical ESPT and proton recombination processes take place on the surface of the microcrystal. The effective concentration of the dopants on the surface is high. If HCl acid is also expelled from the crystal bulk to the surface, then the effective acid concentration becomes very high, and, consequently, the rate of the reaction written below (eq 8) is fast, since it linearly depends on the acid concentration.

$$RO^-* + H^+ \rightarrow ROH \ (g) \qquad (8)$$

The outcome of this photochemical surface reaction analysis is an erroneously large effective proton diffusion coefficient.

The neutron scattering experiment measures the proton hopping time. The strength of the quasi-elastic neutron scattering signal of the excess protons with respect to the total scattering signal is proportional to the fraction of protons participating in diffusion jumps on the time scale of the experiment and independent of the position of the HCl molecules, that is, at the grain boundaries or in the bulk. This means that by using this method we might also be measuring proton hopping on the microcrystal/grain boundaries enriched with HCl. The main result of this article is shown in Figure 5, where a comparison of the hopping times extrapolated from both methods reveals roughly the same values. The hopping times are much shorter than the predicted values from the scientific literature of proton mobility in ice, which are based on conductance measurements. In electric conductance experiments of pure ice the proton concentration is low, $\sim 10^{-13}$ n/N, where n and N are the number of protons and water molecules per unit of volume at ~ 265 K, respectively. It further decreases as the temperature decreases, since its temperature dependence is strong. On top of the above-mentioned difficulties, there are four different conducting species in ice rather than two in liquid water. The concentration of

the D and L orientational defects in pure ice is about one million times higher at 260 K, 10^{-7} n/N. The contact of the metal electrode with the ice and the surface conductivity add to the above difficulties. The literature values of the proton mobility in ice are on the order of the proton mobility in supercooled liquid water, which is roughly half of the value at 295 K. The results of our photochemical experiments at 263 K indicate a value that is 20 times higher than the literature value of proton mobility deduced from the electrical conductance measurements. The temperature dependence of the proton diffusion coefficient derived from the photochemical experiments in the temperature range of 175–268 K conforms with the temperature dependence of the proton conductance measurements in HCl-doped ice of Takei and Maeno.[27,28] However, in their experiments the number of charge carriers per unit of volume was unknown, and, therefore, the proton mobility could not be evaluated. The neutron scattering experiment provides the average proton hopping time at relatively low temperatures. Within a relatively small and reasonable uncertainty, the hopping times of the neutron scattering and the photochemical experiments are in agreement. This correspondence provides strong evidence that at $T > 242$ K protons are indeed highly mobile in the ice I_h structure, roughly 10 times more than in the liquid state at room temperature. What is essentially needed at this stage are quantum mechanical calculations of the proton's movement in ice. If these future calculations show that proton mobility in ice is as high as we found, then a whole new and fascinating field of research should be unlocked.

In liquid water, the QENS signal is mainly determined by very strong (high intensity) slow translational and rotational molecular diffusion from all water molecules. The fast proton hops (similar to those in ice) also exist in liquid water, but it is actually not a single-step process.[39,40] It happens by a transition from the $H_3O^+[3H_2O]$ Eigen proton complex,[41,42] via the $H_5O_2^+$ Zundel-complex, to a $H_3O^+[3H_2O]$ centered on a neighboring water molecule. In the resting period before a transition, there is a distorted hydronium with one of its water ligands at a shorter distance and another at a longer distance than average. The liquid water proton hop occurs on a time scale of femtoseconds. Recently, Voth and co-workers[43,44] employed their multistate empirical valence bond calculation method and ab initio Car–Parrinello molecular dynamics simulations to study aqueous solutions of HCl in the concentration range of 0.5–3 M. In the liquid phase, the hydrated excess protons tend to form metastable contact ion pairs by positioning the hydronium oxygen lone pair sides toward one another. The fast (broad) component in QENS spectra of liquid water is difficult to extract due to its very weak intensity (proportional to the proton defect concentration of the order of 0.1%) compared to the narrow component of molecular diffusion, which is proportional to $\sim 99.9\%$ of the water protons.

■ SUMMARY

We have used the quasi-elastic neutron scattering technique to study HCl-doped ice I_h microcrystalline samples. The scattering signal provided the average hopping time of the proton, τ_{hop}, at several temperatures in the range of 140–195 K. The hopping times range between 8 ps at 195 K to ~ 1100 ps at 140 K. The average activation energy was found to be ~ 17 kJ/mol. These hopping times were compared with previously reported proton diffusion coefficient in ice[21,22] obtained by a photochemical method. The $D_{H^+}^{ice}$ versus $1/T$ plot exhibits a bimodal behavior in the temperature region of 175–265 K. At $T \geq 242$ K, the

temperature dependence of the proton diffusion coefficient, $D_{H^+}^{ice}$, is rather weak, and the activation energy for a proton hop is less than 1 kJ/mol. It is in this temperature range that the proton diffusion coefficient is 10 times larger than that of room temperature liquid water. Below 242 K, the temperature dependence of $D_{H^+}^{ice}$ increases and the activation energy is 22 kJ/mol.[1] We derived the proton hopping time from the proton diffusion coefficient using the Einstein relation (eq 4), in which we set the value of L, the hopping distance, to be 2.75 Å, because this is the distance between oxygen atoms of two adjacent water molecules in ice I$_h$. We find a very good correspondence between the hopping times derived from the photochemical experiments and the ones measured by neutron scattering.

■ ASSOCIATED CONTENT

Ⓢ Supporting Information.   We present the Smoluchowski model to describe the diffusion-assisted irreversible reaction of some photoacids and a table and a figure of the proton hopping times in HCl-doped and methanol-doped ice versus $1/T$. This material is available free of charge via the Internet at http://pubs.acs.org.

■ AUTHOR INFORMATION

Corresponding Author
*E-mail: huppert@tulip.tau.ac.il, phone: 972-3-6407012, fax: 972-3-6407491.

■ ACKNOWLEDGMENT

■ REFERENCES

(1) Uritski, A.; Presiado, I; Erez, Y.; Gepshtein, R.; Huppert, D. *J. Phys. Chem. C* **2009**, *113*, 10285.

(2) Fletcher, N. H. *The Chemical Physics and of Ice*; Cambridge University Press: London, 1970.

(3) Hobbs, P. V. *Ice Physics*; Clarendon Press; Oxford, UK, 1974.

(4) *Physics and Chemistry of Ice*, 5th. ed.; Walley, E., Jones, S. J., Gold, L. W., Eds.; Royal Society of Canada: Ottawa, 1973.

(5) Petrenko, V. F.; Whitworth, R. W. *The Physics of Ice*; Oxford University, Press: Oxford, UK, 1999.

(6) Bolton, K.; Pettersson, J. B. C. *J. Am. Chem. Soc.* **2001**, *123*, 7360.

(7) Jaccard, C. *Ann. N.Y. Acad. Sci.* **1965**, *125*, 390.

(8) Bjerrum, N. *Science* **1952**, *115*, 385.

(9) Kobayashi, C.; Saito, S.; Ohmine, I. *J. Chem. Phys.* **2001**, *115*, 4742.

(10) Podeszwa, R.; Buch, V. *Phys. Rev. Lett.* **1999**, *83*, 4570.

(11) (a) Eigen, M. Proton Transfer. *Angew. Chem., Int. Ed* **1964**, 3, 1. (b) Eigen, M.; Kruse, W.; Maass, G.; De Maeyer, L. *Prog. React. Kinet.* **1964**, *2*, 285.

(12) Eigen, M.; de Maeyer, L. In *The Structure of Electrolytic Solutions*; Wiley: New York, 1959; p 64, et seq.

(13) Kelly, I. J.; Salomon, R. R. *J. Phys. Chem.* **1969**, *50*, 75.

(14) Camplin, G. C.; Glen, J. W. *Physics and Chemistry of Ice*, 5th ed.; Walley, E., Jones, S. J., Gold, L. W., Eds.; Roy. Soc. Canada: Ottawa, 1973; p 256.

(15) Kunst, M.; Warman, J. M. *J. Phys. Chem.* **1983**, *87*, 4093.

(16) Onsager, L.; Runnels, L. K. *J. Chem. Phys.* **1969**, *50*, 1089.

(17) Nagle, J. F. *J. Phys. Chem.* **1983**, *87*, 4086.

(18) Demiridjian, B.; Ferry, D.; Suzanne, J.; Toubin, C.; Picaud, S.; Hoang, P. N. M.; Girardet, C. *J. Chem. Phys.* **2002**, *116*, 5143.

(19) Kang, H. *Acc. Chem. Res.* **2005**, *38*, 893.

(20) Uras-Aytemiz, N.; Joyce, C.; Devlin, J. P. *J. Phys. Chem. A* **2001**, *105*, 10497.

(21) Park, S. C.; Jung, K. H.; Kang, H. *J. Chem. Phys.* **2004**, *121*, 2765.

(22) Wooldridge, P. J.; Devlin, J. P. *J. Chem. Phys.* **1988**, *88*, 308.

(23) Fisher, M.; Devlin, J. P. *J. Phys. Chem.* **1995**, *99*, 11584.

(24) Everest, M. A.; Pursell, C. J. *J. Chem. Phys.* **2001**, *115*, 9843.

(25) Cowin, J. P.; Tsekouras, A. A.; Iedema, M. J.; Wu, K.; Ellison, G. B. *Nature* **1999**, *398*, 405.

(26) Ayotte, P.; Rafiei, Z.; Porzio, F.; Marchand, P. *J. Chem. Phys.* **2009**, *131*, 124517.

(27) Takei, I.; Maeno, N. *J. Phys. Chem.* **1984**, *81*, 6186.

(28) Takei, I.; Maeno, N. *J. Phys. (Paris)* **1987**, 48, Colloque C1, 121.

(29) Cohen, B.; Huppert, D.; Agmon, N. *J. Phys. Chem. A* **2001**, *105*, 7165.

(30) Pang, X. F.; Feng, Y. P. *Chem. Phys. Lett.* **2003**, *373*, 392.

(31) Mamontov, E.; Zamponi, M.; Hammons, S.; Keener, W. S.; Hagen, M.; Herwig, K. W. *Neutron News* **2008**, *19*, 22.

(32) Uritski, A.; Presiado, I.; Huppert, D. *J. Phys. Chem. C* **2009**, *113*, 7870.

(33) Uritski, A.; Presiado, I.; Erez, Y.; Gepshtein, R.; Huppert, D. *J. Phys. Chem. C* **2009**, *113*, 12901.

(34) Agmon, N. *J. Phys. Chem. A* **2005**, *109*, 13.

(35) Rips, I.; Jortner, J. *J. Chem. Phys.* **1987**, *87*, 2090.

(36) Szabo, A. *J. Phys. Chem.* **1989**, *93*, 6929.

(37) Collins, F. C.; Kimball, G. E. *J. Colloid Sci.* **1949**, *4*, 425.

(38) See Table 5.2 in ref 5.

(39) Lapid, H.; Agmon, N.; Petersen, M. K.; Voth, G. A. *J. Chem. Phys.* **2005**, *122*, 014506.

(40) Markovitch, O.; Chen, H.; Izvekov, S.; Paesani, F.; Voth, G. A.; Agmon, N. *J. Phys. Chem. B* **2008**, *112*, 9456.

(41) Eigen, M. *Angew. Chem., Int. Ed.* **1964**, *3*, 1.

(42) Zundel, G. *The Hydrogen Bond, Recent Developments in Theory and Experiments*; Schuster, P., Zundel, G., Sandorfy, C., Eds.; North Holland: Amsterdam, 1976; pp 687−766.

(43) Wang, F.; Izvekov, S.; Voth, G. *J. Am. Chem. Soc.* **2008**, *130*, 3120.

(44) Xu, J.; Izvekov, S.; Voth, G. *J. Phys. Chem. B* **2010**, *114*, 9555.

10251

dx.doi.org/10.1021/jp2008094 |*J. Phys. Chem. C* 2011, 115, 10245–10251